ISSN 2616-5880 Vol. 4, Issue 4: 1-6, DOI: 10.25236/AJMC.2023.040401

A.C. impedance of γ-$LiAlO_2$ film prepared by laser CVD

Chen Chi[1,a,*]

[1]*School of Chemical Engineering and Pharmacy, Wuhan Institute of Technology, Wuhan, China*
[a]*15327326216@163.com*
[*]*Corresponding author: Chen Chi*

Abstract: *(110)-oriented γ-$LiAlO_2$ film consisting of granular grains was prepared by laser CVD. The complex impedance of polycrystalline γ-$LiAlO_2$ film showed dispersions due to bulk, grain-boundary and electrode. Temperature dependence of the electrical conductivity for γ-$LiAlO_2$ film, polycrystalline sintered sample and single crystals obeyed Arrhenius behaviour. The electrical conductivity (σT) of the γ-$LiAlO_2$ film reached 196 $S{\cdot}m^{-1}{\cdot}K$ at 1173 K, nearly 5 times higher than the maximum value of γ-$LiAlO_2$ single crystals and polycrystalline sintered samples.*

Keywords: *γ-$LiAlO_2$; electrical conductivity; impedance; arrhenius behaviour*

1. Introduction

γ-$LiAlO_2$ has a wurtzite structure in a tetragonal cell ($P4_12_12$; a = 5.17 nm and c = 6.295 nm), which is composed of Al- and Li-centered tetrahedra. Each tetrahedron shares one of its edges with another tetrahedron of different kind and each vertex of every tetrahedron is shared with two additional tetrahedra. γ-$LiAlO_2$ has many applications including lattice-match substrate for GaN semiconductor [1], electrolyte support for molten carbonate full cell (MCFC) [2], tritium breeding material for fusion reactor [3] and piezoelectric material for surface acoustic wave (SAW) devices [4]. The tritium release property of γ-$LiAlO_2$ was closely associated with lithium ionic conduction [5-8].

Solid state reaction [9, 10] and wet-chemical method (i.e., sol-gel) [11-13] have been applied to prepare γ-$LiAlO_2$ samples. However, no study on the preparation and the electrical conduction of γ-$LiAlO_2$ film was reported to date. In the previous study, we successfully obtained (004)-oriented γ-$LiAlO_2$ film by laser CVD. At present, (110)-oriented γ-$LiAlO_2$ film was prepared and the electrical conductivities of γ-$LiAlO_2$ film, polycrystalline sintered sample and single crystals with different orientations were investigated.

2. Experimental details

The schematic of Laser CVD apparatus was shown elsewhere [14]. A continuous wave diode laser (InGaAlAs, wavelength: 808 nm) was employed with laser power output (P_L) from 100 to 200 W and irradiation spot size of 15 mm in diameter. AlN substrate (10 mm × 10 mm × 1mm) was put on a hot stage that was pre-heated at 873 K (T_{pre}). The deposition temperature (T_{dep}) was measured by a thermocouple beneath the substrate. The vaporization temperature (T_{vap}) of Al $(acac)_3$ (acac: acetylacetonate) precursor was fixed at 443 K, whereas that of Li(dpm) (dpm: dipivaloymethanate) precursor was changed from 513 to 553 K. The molar ratio of evaporated Li to Al precursors ($R_{Li/Al}$) was regulated by changing the T_{vap} of Li (dpm) precursor. The precursor vapor and O_2 gas were separately introduced into the chamber through a double-tube nozzle. The flow rates of Ar carrier gas for each precursor and O_2 gas were fixed at 8.3×10^{-7} and 1.7×10^{-6} $m^3\ s^{-1}$, respectively. The temperature of all the gas lines was maintained at 553 K to prevent the condensation of precursor during the transportation. The total chamber pressure (P_{tot}) was kept at 200 Pa. The deposition time was 600 s.

The deposition rate (R_{dep}) was calculated from the thickness increase of films per deposition time. The crystalline phase of Li-Al-O films was examined by X-ray diffraction (XRD; Rigaku: RAD-2C). The microstructure was observed by scanning electron microscopy (SEM; Hitachi: S-3100H).

ISSN 2616-5880 Vol. 4, Issue 4: 1-6, DOI: 10.25236/AJMC.2023.040401

The impedance measurements were carried out in the temperature range of 773 to 1173 K in air using a Solartron 1296 frequency analyzer coupled to a 1286 dielectric interface over the frequency range 10^{-2} to 10^{7} Hz. Platinum and gold were used as the bottom and upper electrodes, respectively. Before each impedance measurement the cell was kept at the testing temperature for at least 30 min to allow thermal equilibration.

3. Experimental details

Figure 1 shows XRD pattern of Li-Al-O film prepared at $R_{Li/Al}$ = 3.1, T_{dep} = 1175 K (P_L = 100 W) and P_{tot} = 200 Pa. Relative intensity of the (110) peak at 24.3° was significantly higher than that of a powder pattern (JCPDF#75-0905) and the other peaks, even including the strongest peak (101) in powder, were not conspicuous, implying (110) orientation.

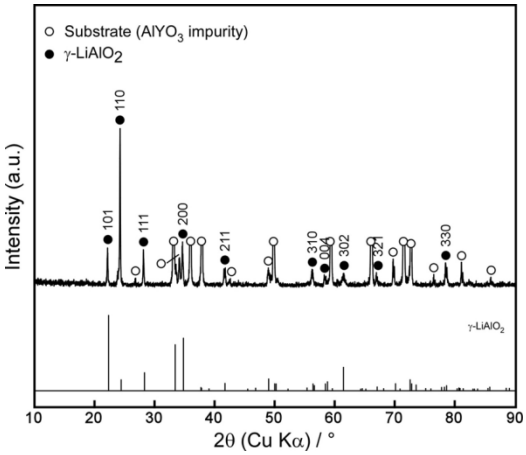

Figure 1: XRD pattern of Li-Al-O film prepared at T_{dep} = 1175 K (P_L = 100 W), $R_{Li/Al}$ = 3.1 and P_{tot} = 200 Pa.

Figure 2 shows the surface and cross section of (110)-oriented γ-$LiAlO_2$ film. At $R_{Li/Al}$ = 3.1, T_{dep} = 1175 K and P_{tot} = 200 Pa, γ-$LiAlO_2$ film consisted of granular grains (Fig. 2(a)). The film had columnar cross section (Fig. 2(b)). Deposition rate (R_{dep}) of the film was calculated from the thickness of cross section. The R_{dep} of (110)-oriented film reached 50 μm h^{-1}.

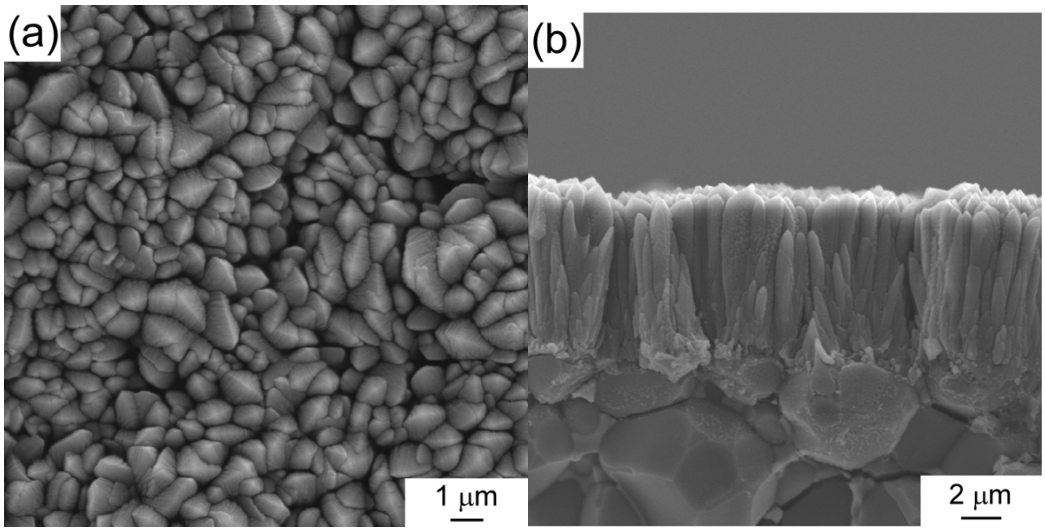

Figure 2: Surface and cross section images of (110)-oriented γ-$LiAlO_2$ film.

Figure 3 shows the complex impedance plots of γ-$LiAlO_2$ film (a) and single crystal sintered sample (b) at 873 K. Fig. 3(a') presents the amplified high-frequency area of (a). The complex impedance of γ-$LiAlO_2$ film consisted of a semicircle at high frequency, an arc appearing from 10^2 – 10^5 Hz and an inclined straight line at low frequency while that of γ-$LiAlO_2$ single crystal sintered sample had only a semicircle and spike. It could be deduced that the electrical processes arise basically due to the

ISSN 2616-5880 Vol. 4, Issue 4: 1-6, DOI: 10.25236/AJMC.2023.040401

contribution from bulk and electrolyte/electrode interface for γ-$LiAlO_2$ single crystal and additional grain boundary effect for γ-$LiAlO_2$ polycrystalline film. The complex impedance of γ-$LiAlO_2$ single crystal was fitted by an equivalent circuit composed of bulk resistance (R_b), constant phase element of bulk (CPE_b) and Warburg impedance (Z_w) while that of γ-$LiAlO_2$ film was modeled in terms of an equivalent electrical circuit comprising of a series combination of two parallel *R*-*CPE* and one single Z_w. Mathematically, a *CPE* impedance can be given by

$$\frac{1}{Z_{CPE}} = Y = Q^0(j\omega)^n \tag{1}$$

where ω is the angle frequency and Q^0 has the numerical value of the admittance (1/|ZCPE|) at ω=1 rad/s. The R_b denotes bulk resistance and CPE_b covers geometry capacity and effect of dipolar relaxation [15]. The parallel R_{gb}-CPE_{gb} reflects the effect of grain boundary on electrical processes. The high-frequency semicircle slightly depressed reflects the combination of R_b and CPE_b. The Warburg equation is shown as follow

$$Z_w = \sigma\omega^{-\frac{1}{2}}(1-j)tanh(\delta\left(\frac{j\omega}{D}\right)^{\frac{1}{2}}) \tag{2}$$

where σ is the Warburg coefficient, δ Nernst diffusion layer thickness and D the average value of the diffusion coefficients of the diffusing species. The spike can be explained with Z_w, meaning the presence of ionic diffusion. The low-frequency end of the semicircle located in the high-frequency range and Z'-axis intersect at R_b. The R_b of film was obviously smaller than that of single crystal.

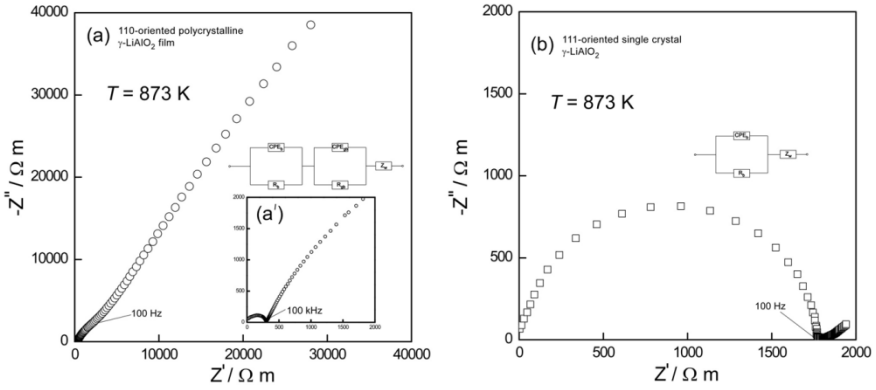

Figure 3: Complex impedance of γ-$LiAlO_2$ film (a) and single crystal (b) at 873 K.

Increasing temperature to 973 K, the high-frequency semicircle tended to vanish and the subsequent arc appeared at frequency from 10^3 – 2×10^5 Hz in the impedance pattern of the γ-$LiAlO_2$ film (Fig. 4(a)), indicating electrical relaxation occurring at higher frequency with increasing temperature. For single crystal sintered sample, the complex impedance plot keeps the same components as that at 873 K (Fig. 4(b)).

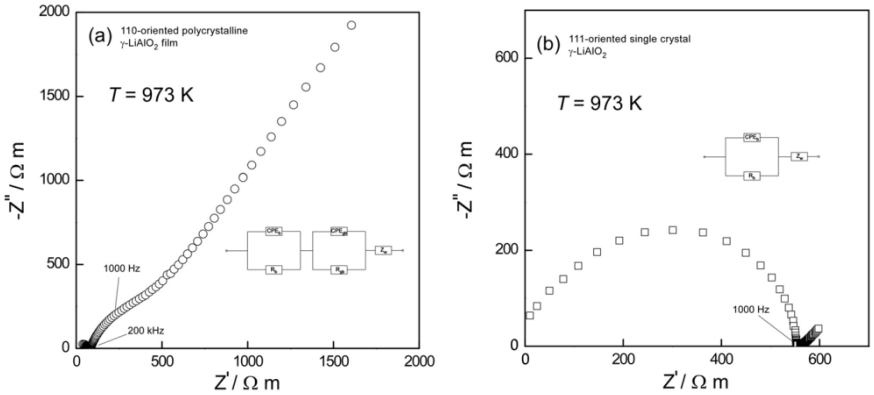

Figure 4: Complex impedance of γ-$LiAlO_2$ film (a) and single crystal (b) at 973 K.

Figure 5 (a) and (b) show the real and imaginary parts of modulus respectively at different temperatures for γ-$LiAlO_2$ film. It is observed in Fig. 5(a) that real modulus M' shows dispersion as the frequency is increased. The small value of M' in the low frequency region facilitates the migration of

ISSN 2616-5880 Vol. 4, Issue 4: 1-6, DOI: 10.25236/AJMC.2023.040401

ion conduction. It is also observed in Fig. 5(b) that the imaginary modulus M" exhibits a single relaxation peak centered at the dispersion region of M'. As the temperature is increased the movement of the charge carriers becomes faster, leading to deceased relaxation time, with a consequent shift of the peak value in M" toward higher frequencies. This behavior suggests that the relaxation is thermally activated, and charge carrier hopping is taking place.

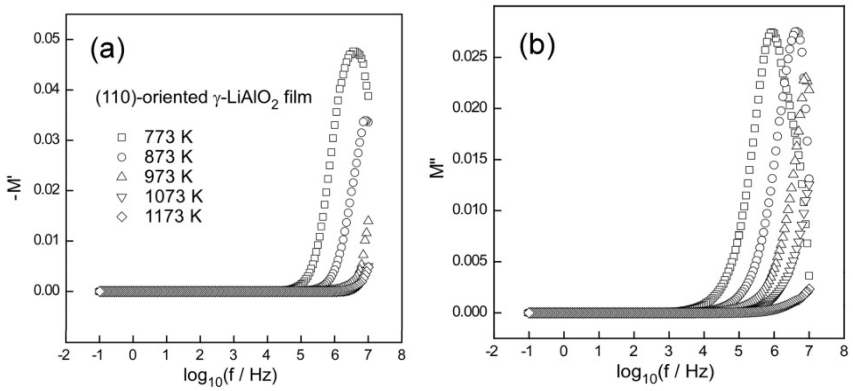

Figure 5: Frequency dependence of (a) real part (M') and (b) imaginary part (M") of modulus spectra at various temperatures for γ-LiAlO₂ film.

The conductivity relaxation frequency f_m corresponds to M''_{max}. The scaling behavior of the modulus spectra provides an insight into the temperature dependence of the relaxation dynamics. We have scaled the modulus spectra for M'' at different temperatures for γ-$LiAlO_2$ film in Fig. 6(a). The scaling process has been performed by dividing M'' with M''_{max} while the frequency axis is scaled by the relaxation frequency f_m. The overlap of the spectra at different temperatures on a single master curve indicates that the dynamical processes occurring at different temperatures are almost independent of temperature. The scaling results for γ-$LiAlO_2$ film, polycrystalline sintered sample and single crystal at a particular temperature are shown in Fig. 6(b). We note that all the modulus spectra are scaled to a common master curve. These results suggest that the relaxation dynamics of charge carrier in γ-$LiAlO_2$ film, polycrystalline sintered sample and single crystal follows a common mechanism throughout the entire temperature and the effect of grain-boundary is ignored.

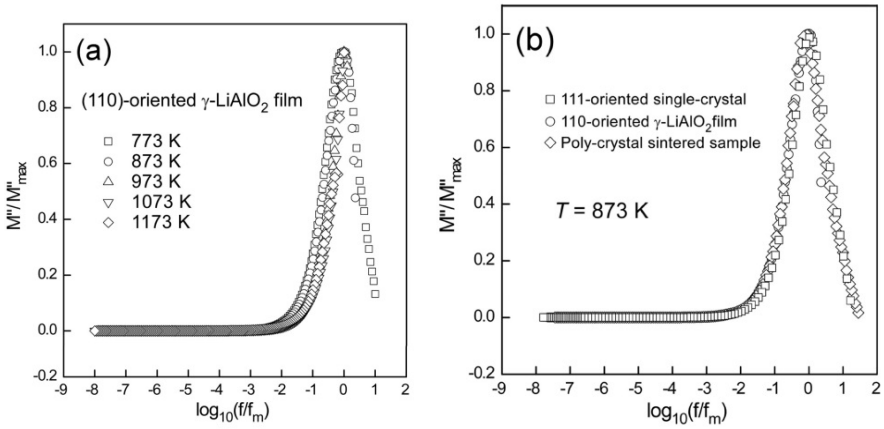

Figure 6: Plots of M"/M"max versus $log_{10}(f/f_m)$ (a) at different temperatures for γ-$LiAlO_2$ film and (b) the same plot at 873 K for γ-$LiAlO_2$ sintered sample, single crystal and film.

The R_b at every temperature investigated was formally converted to an electrical conductivity (σ), using the relation [16]

$$\sigma = d/AR_b \tag{3}$$

where d is the sample thickness and A the electrode area of sample surface. Figure 7 shows temperature dependence of electrical conductivity in the form of σT (where T is the temperature) for γ-$LiAlO_2$ film, polycrystalline sintered sample and single crystals. The increase of electrical conductivity with rise in temperature indicated that electrical conduction in γ-$LiAlO_2$ materials was a thermally activated process. The σT of γ-$LiAlO_2$ film was almost the same as those of its single crystals

ISSN 2616-5880 Vol. 4, Issue 4: 1-6, DOI: 10.25236/AJMC.2023.040401

and polycrystalline sintered sample at room temperature. With increasing temperature, the σT of γ-$LiAlO_2$ film increased more rapidly and became 5 times higher than those of its single crystals and polycrystalline sintered sample above 973 K. For example, at 1173 K, the σT of (110)-oriented γ-$LiAlO_2$ film reached 196 $S \cdot m^{-1} \cdot K$ and the maximum σT for γ-$LiAlO_2$ single crystals and polycrystalline sintered sample was 42 $S \cdot m^{-1} \cdot K$. Compared with polycrystalline sintered samples reported previously, γ-$LiAlO_2$ film also showed superior electrical conductivity. By LCVD, γ-$LiAlO_2$ films were prepared at $R_{Li/Al} > 1.0$, more than the ratio of Li/Al in its formula. And (110)-oriented γ-$LiAlO_2$ films were obtained at higher $R_{Li/Al}$. Although only γ-$LiAlO_2$ was identified by XRD in the (110)-oriented film, the $R_{Li/Al}$ was detected to be approximately 2.0 by electron energy loss spectroscopy (EELS). The high electrical conductivity of (110)-oriented γ-$LiAlO_2$ film may be related to the excessive Li content in the material.

The dependence of logarithm of σT on inverse of temperature (1000/T) showed a typical Arrhenius behavior (a linear relationship between log(σT) and 1/T) and obeyed the traditional Arrhenius equation

$$\sigma T = \sigma_0 exp(-\frac{E_a}{kT}) \quad (4)$$

where E_a is the activation energy for conduction, and the pre-exponential factor (σ_0) is a material constant. Calculated from the relation, the activation energy (E_a) of γ-$LiAlO_2$ polycrystalline sintered sample and film is 1.18 eV, slightly higher than those of single crystals (1.02 eV).

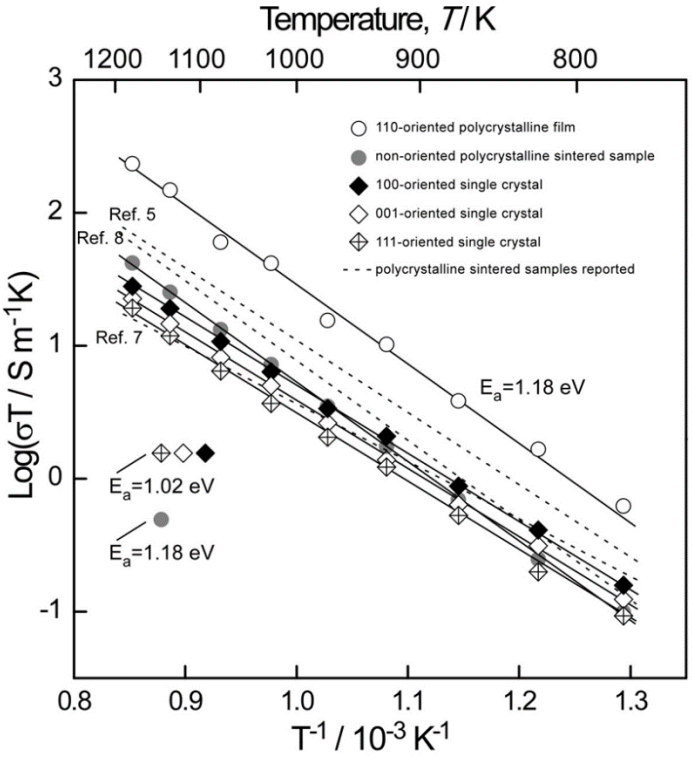

Figure 7: Temperature dependence of electrical conductivity (σT) of γ-$LiAlO_2$ polycrystalline film, sintered samples and single crystals.

4. Conclusions

(110)-oriented γ-$LiAlO_2$ films were obtained by laser chemical vapor deposition at T_{dep} = 1050 – 1250 K, $R_{Li/Al}$ = 0.9 – 10.2 and P_{tot} = 200 Pa. The (110)-oriented film showed granular surface and columnar cross-section. The AC impedance of γ-$LiAlO_2$ polycrystalline film and sintered sample show two curve dispersions due to bulk and grain-boundary respectively and a spike attributed to electrolyte/electrode surface. A scaling of the modulus spectra of γ-$LiAlO_2$ film, polycrystalline sintered sample and single crystals at different temperatures reveals that the electrical process follows the same mechanism throughout the entire temperature and the effect of grain-boundary is not evident. The electrical conductivity of γ-$LiAlO_2$ film is 5 times higher than those of γ-$LiAlO_2$ single crystals and polycrystalline sintered sample at the same temperature.

ISSN 2616-5880 Vol. 4, Issue 4: 1-6, DOI: 10.25236/AJMC.2023.040401

Acknowledgements

This work was supported by the project of Research on Preparation and Properties of Ceramic Electrolyte BASE (No. 005351), financed by Education Department of Hubei Province, China.

References

[1] M.M.C. Chou, H.C. Huang, Y.F. Chang, et al. Defects and acoustic properties of $LiAlO_2$. Appl. Phys. Lett., 2006, 88:161906.
[2] A.N. Webb, J.W.B. Mather, R.M. Suggitt. Studies of the Molten Carbonate Electrolyte Fuel Cell. J. Electrochem. Soc., 1965, 112: 1059-1063.
[3] J.A. Shearer, S.W. Tam, C.E. Johnson. Tritium diffusion in lithium oxide solid breeder materials. Conference: ANS annual meeting, Detroit, MI, USA, 12 Jun 1983, 36:1066.
[4] A.V. Sotnikov, H. Schmidt, M. Weihnacht, E.P. Smirnova, T.Y. Chemekova, Y.N. Makarov. Elastic and piezoelectric properties of AlN and $LiAlO_2$ single crystals. IEEE Trans. Ultrason. Ferroelectr. Freq. Control, 2010, 57: 808-811.
[5] F. Alessandrini, C. Alvani, S. Casadio, M.R. Mancini, C.A. Nannetti. In-situ tritium release (CORELLI-2 experiment) and ex-reactor ionic conductivity of substoichiometric $LiAlO_2$ breeder ceramics. J. Nucl. Mater, 1995, 224: 236-244.
[6] C. Alvani, S. Casadio, L. Lorenzini, G. Brambilla. FABRICATION OF POROUS $LiAlO_2$ CERAMIC BREEDER MATERIAL. Fusion Technol., 1986, 10: 106-112.
[7] H. Ohno, S. Konishi, T. Nagasaki, T. Kurasawa, H. Katsuta, H. Watanabe. Correlation behavior of lithium and tritium in some solid breeder materials. J. Nucl. Mater, 1985, 133:181-185.
[8] Z. Wen, Z. Gu, X. Xu, X. Zhu. Research on the preparation, electrical and mechanical properties of γ-$LiAlO_2$ ceramics. J. Nucl. Mater., Part B 2004, 329: 1283-1286.
[9] M.A. Valenzuela, J. Jimenez-Becerril, P. Bosch, S. Bulbulian, V.H. Lara. Sol-gel synthesis of lithium aluminate. J. Am. Ceram. Soc., 1996, 79: 455-460.
[10] T. Frianeza-Kullberg, D. Mcdonald, K. Davis. Effect of temperature on formation of lithium aluminate particles by calcination. Ceram. Trans., 1990, 12: 147.
[11] C. Alvanic, S. Casadio. A wet method to prepare gamma lithium aluminate with 1:1 ratio of Li/Al. EP235099, 1987.
[12] K.W Sang, S Binpark, et al. Research on electrical properties of $LiAlO_2$ ceramic. J. Nucl. Mater., 1998, 257: 172.
[13] L.M. Carrera, J. Jimenez-Becerril, P. Bosch, S. Bulbulian. Effect of synthesis techniques on crystallite size and morphology of lithium aluminate. J. Am. Ceram. Soc., 1995, 78: 933-938.
[14] C. Chi, H. Katsui, R. Tu, T. Goto. Preparation of Li–Al–O films by laser chemical vapor deposition. Mater. Chem. Phys., 2014, 143: 1338-1343.
[15] X. Qian, N. Gu, Z. Cheng, X. Yang, E. Wang, S. Dong. Methods to study the ionic conductivity of polymeric electrolytes using a.c. impedance spectroscopy. J. Solid State Electrochem., 2001, 6: 8-15.
[16] J. Gong, Y. Li, Z. Tang, Y. Xie, Z. Zhang. Temperature-dependence of the lattice conductivity of mixed calcia/yttria-stabilized zirconia. Mater. Chem. Phys., 2002, 76:212-216.